International Journal of Mathematical Analysis and Modelling

(Formerly Journal of the Nigerian Society for Mathematical Biology)

Volume 8 Issue 2, 2025

ISSN (Print): 2682 - 5694
ISSN (Online): 2682 – 5708
www.tnsmb.org

Heat and mass distribution by mixed convection in an unsteady power law fluid over an accelerated riga plate under the influence of heat generation/absorption and thermal radiation

A.A. Adeyemi[*†], B.I. Olajuwon[‡], L.O. Sogbetun[§] M.O. Iyoko[¶], M.T. Raji[‖], O. Fagbemiro[**] and I.A. Adejumobi[††]

Abstract

The significance of heat generation/absorption, thermal radiation, inclination angle and chemical reaction on the convective heat and mass transfer in a power law fluid over an accelerated Riga plate is examined. This study investigates the non-Newtonian power law index for the cases when (pseudo-plastic fluid), and (dilatant fluid). The Grinberg term incorporated into the momentum equation is utilized to express the Riga plate. By employing suitable transformation technique, related non-linear partial differential equations formulated are converted to ordinary differential equations. The resulting similarity equations are solved numerically by employing shooting method embedded in Matlab computational software. Graphs are utilized to illustrate the impact of fluid variables entering the velocity, temperature, and concentration profiles. Further, numerical outcomes of the combined effects of thermal radiation, chemical reaction and heat generation on the skin friction coefficients, heat transfer rate and mass transfer rate are tabulated and analysed. The results disclose contribution of sundry parameters on the fluid flow, mass and heat transfers.

Keywords and phrases: mixed convection; power-law fluid; Riga plate; heat generation/absorption; thermal radiation

1 Introduction

Recent years have seen a significant increase in interest in the study of non-Newtonian fluids. One major explanation for this could be because their high demands in industrial and engineering processes. Non-Newtonian fluids such molten plastics, pulps, slurries, paints, pharmaceutical formulations, cosmetics and toiletries, suspensions and dispersion, polymer solutions, melts and emulsions are manufactured in increasing amounts for industrial use. Majority of these liquids which are non-Newtonian fluids, exhibit a complex rheological behaviour which is deviated from the traditional Newton's law of viscosity which states that the stress tensor is directly proportional to the deformation tensor. Numerous models have been put out to explain the peculiarity of these fluids. Among the most widely accepted of these models is the power-law model found in Schlichting [1], in which shear stress varies according to a power-law function of strain. Zhang et al. [2] examined the flow and heat transport in a power law fluid across

[*]Corresponding Author; E-mail: funaabfluidmechanicsresearch@gmail.com adeyemiazeez4137@gmail.com
[†]Department of Mathematics, Federal University of Agriculture, Abeokuta, Nigeria
[‡]Department of Mathematics, Federal University of Agriculture, Abeokuta, Nigeria; E-mail: olajuwonbi@funaab.edu.ng
[§]Department of Mathematics, Federal University of Agriculture, Abeokuta, Nigeria; E-mail: sogbetunlateef@gmail.com
[¶]Department of Mathematics, Federal University of Agriculture, Abeokuta, Nigeria; E-mail: iyokomo@funaab.edu.ng
[‖]Department of Mathematics, Federal University of Agriculture, Abeokuta, Nigeria; E-mail: rajimt@funaab.edu.ng
[**]Department of Mathematics, Federal University of Agriculture, Abeokuta, Nigeria; E-mail: fagbemiroo@funaab,edu.ng
[††]Department of Mechanical Engineering, Federal University of Agriculture, Abeokuta, Nigeria; E-mail: adejumobiia@funaab,edu.ng

a stretching sheet using a numerical approach. Bharti et al. [3] investigated the forced convection heat and mass transfer of a steady power law fluid past a heated cylinder. Hassan et al. [4] and Donald [5] separately studied the boundary layer equations involving power law fluid over a nonlinear stretching sheet. The flow and convection heat transfer via a vertical plate with heat generation in a pseudoplastic power law fluid was investigated by Olajuwon [6]. Again, Olajuwon and Oyelakin [7] analysed the role of thermo and thermal diffusion on the convection heat and mass diffusion in power law fluid with uniform relaxation time over a porous medium.

Significance of heat absorption/generation parameter in influencing thermofluid and mass diffusion flow of a viscous, incompressible, and electrically conducting fluid has been acknowledged in literature. Its impact is vital in metallurgy, astronomy, geophysics, electronics, aeronautics, oil industry etc. Effect of magnetic field and heat generation/absorption on convective heat and mass transfer was studied by Chamkha and Khaled [8]. The research indicated that higher heat absorption raises the heat transfer rate. Research on unsteady MHD flow over a semi-infinite vertical porous plate under the influence of heat absorption was conducted by Chamkha [9]. The findings revealed that augmented heat absorption parameter reduces the Nusselt number, and an increase in Schmidt number reduces Sherwood number. Asimoni et al. [10] studied the influence of heat absorption and chemical reaction effects on the two-dimensional MHD convective flow of a non-Newtonian nanofluid in a lid-driven cavity. The temperature distribution was found to be improved by the heat absorption parameter. Reddy et al. [11] investigated the impact of chemical reaction and radiation on MHD stagnation point flow past a stretching surface. The findings showed that an augmented thermal radiation widens thermal boundary layer thickness while higher heat absorption produces reverse effect. Also, the species concentration falls when the chemical reaction parameter is raised. Analytical solutions for time-dependent magnetic field convection in a heat-absorbing fluid flow past a ramping plate were examined by Nandkeolyar et al. [12]. They noted that heat absorption causes the liquid temperature and fluid flow to decline but raises the shear stress and the rate of heat transfer at the plate.

Lately, research on electromagnetohydrodynamics has been on an increase due to its numerous scientific and technological applications particularly in nuclear reactors and submarines. Riga plate also known as electromagnetic actuator was invented by Gailitis and Lielausis [13]. It is a configuration of alternating electrodes and permanent magnets fixed on a surface which generates a Lorentz force. Riga plate is effective in reducing the influence of turbulence in submarines and thereby preventing the separation of the boundary layer and reducing viscosity and pressure drag (Ahmad et al., [14]). The flow of a weakly electrically conducting fluid along a flat Riga plate was investigated initially by Pantokratoras and Magyari [15]. Later, Magyari and Pantokratoras [16] expanded this analysis to incorporate the effect of Lorentz force on an opposing and assisting low viscous fluid. In the meantime, a study on the flow of nanofluid induced by a Riga plate experiencing variable thickness under convective surface wall conditions was carried out by Hayat et al. [17] using the homotopy analysis method. Ramesh et al. [18] in another work, extended the work of Hayat et al. [17] by incorporating non-Newtonian Maxwell nanofluid into the model. The movement of a hydromagnetic dusty fluid over a Riga plate was recently analysed by Prasannakumara et al. [19]. The authors concluded that the thermal field was diminishing as a result of an increase in the modified Hartmann number. Similarly, Rasool and Zhang [20] studied the influence of chemical reaction and thermal radiation on the Powell-Eyring nanofluid flow over a Riga plate subject to convective surface conditions.

Radiation is a fundamental aspect in thermal distribution, influencing the temperature profile and the heat transfer. Radiation plays a crucial role in thermal systems, and its emission is subject to the temperature of the object. The significance of radiative heat transfer has been found in industrial processes such as gas turbines, chemical engineering, energy-conversion devices, nuclear power plants, metallurgical processes, space technology, solar and power technology, and so on. Understanding and accounting for the effects of thermal radiation are crucial for the construction of advanced energy conversion systems operating at high temperatures, like in astrophysical flows, missile re-entry rocket combustion chambers, heat exchangers, and so on. Hayat et al. [21] studied the influence of heat source/sink on an MHD Maxwell nano liquid flow. Rashad [22] investigates the effects of radiation and slip on MHD flow. Lopez et al. [23] examined the MHD nanoliquid flow under the influence of radiation and convective conditions. The effect of heat radiation on non-Newtonian nanofluid flow with entropy rate was examined by Khan et al. [24]. Bilal et al. [25] investigate the heat transport analysis in hydromagnetic radiative flow of Williamson nanoliquid. Daniel et al. [26] analysed the impact of thermal radiation and viscous dissipation on the time-dependent and chemically reactive magnetohydrodynamic (MHD) flow.

This paper examines heat and mass diffusion by mixed convection in an unsteady power law fluid over an accelerated Riga plate which to the best of my knowledge has never be done. The main objectives of this study are to investigate heat and mass transfer of non-Newtonian fluid for all cases of the power law exponent when (pseudo-plastic fluid), and (dilatant fluid), analyse the combined influence of nonlinear thermal radiation, heat source, inclination angle, and chemical reaction parameter on the flow over Riga plate, and discuss the fluid flow rate, mass, and heat transfers with respect to entering fluid parameters in the model. The novelty of this current work can be found in the above-outlined objectives. This study extends its analysis beyond the pseudo-plastic non-Newtonian fluid commonly found in the literature to dilatant non-Newtonian fluid. Also, examining the impact of thermal radiation and heat absorption/generation on the convective flow of a power law fluid over an unevenly inclined Riga plate is greatly important. To the best of our knowledge, this study of the combined effects of heat generation/absorption, thermal radiation, inclination angle, and chemical reaction on heat and mass transfer in an unsteady power law fluid over an inclined Riga plate is a novel work and has never been done by any researcher. The dimensionless governing equations are obtained through adequate transformations. Matlab solver bvp4c is employed to obtain the numerical solutions of the problem. The consequences of relevant fluid parameters entering the boundary layer problem are presented through flow, heat, and mass profiles for pseudo-plastic fluid, and dilatant fluid. Tabular presentations of mass transfer, skin friction, and rate of heat transfer are also made available.

2 Methodology/Model formulation

The problem of heat and mass diffusion by mixed convection in an unsteady power law fluid over an accelerated Riga plate under the influence of heat generation/absorption, thermal radiation, inclination angle and chemical reaction is examined. The fluid's shear stress obeys Ostwald-de Waele rheological model $\tau = \mu\left(\left|\frac{\partial u}{\partial y}\right|^{n-1}\frac{\partial u}{\partial y}\right)$ where $0 < n < 1$ connotes pseudo-plastic non-Newtonian fluids, $n = 1$ correspond to Newtonian fluid while $n > 1$ signifies dilatant fluids. The symbols U_ω, T_ω and C_ω represent the surface velocity, temperature and concentration of the inclined plate respectively with an inclination angle $0 \leq \phi \leq \frac{\pi}{2}$ between the plate and the horizontal direction. The dimensional coordinate of the plate is chosen along the (x, y) with the corresponding velocity components (u, v). Based on the illustration in Figure 1 below, the x axis represents the flow direction, and the y axis is normal to it. The Riga plate is made up of electrodes and permanent magnets of width S in size that are fixed alternatively on the sheet. The roles of pertinent fluid variables are accounted for in the flow, heat and species equations. Applying Boussinesq's approximation, the time-dependent governing equations for the model, including the continuity, momentum, energy, and concentration equations are

$$\frac{\partial u}{\partial x} + \frac{\partial v}{\partial y} = 0 \tag{1}$$

$$\frac{\partial u}{\partial t} = -\nu\frac{\partial}{\partial y}\Big[-\frac{\partial u}{\partial y}\Big]^n + g\lambda(T - T_\infty)\cos\phi + g\beta(C^* - C_\infty)\cos\phi + \frac{\nu}{k}u^n + \frac{\pi J_0 m_0}{8\rho}\exp^{-\frac{\pi}{l}y} \tag{2}$$

$$\frac{\partial T}{\partial t} = \alpha\frac{\partial^2 T}{\partial y^2} - \frac{\alpha}{k}\frac{\partial q_r}{\partial y} + \frac{\alpha}{k}Q_1(T - T_\infty) \tag{3}$$

$$\frac{\partial C^*}{\partial t} = D\frac{\partial^2 C^*}{\partial y^2} - \Gamma_1(C^* - C_\infty) \tag{4}$$

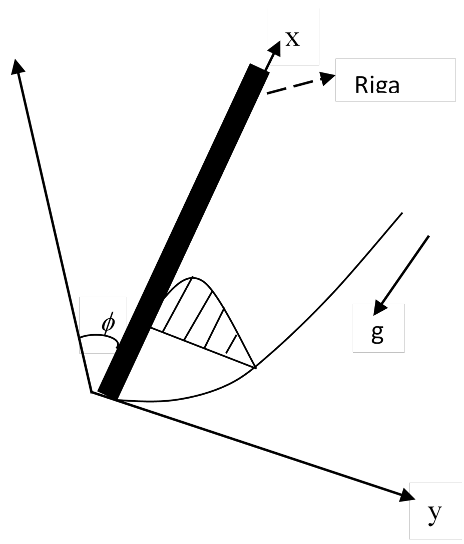

Figure 1: The flow diagram

The appropriate boundary conditions are:

$$u = U_\omega, \quad T = T_\omega, \quad C^* = C_\omega, \quad \text{at} \quad y = 0, \quad t = 0 \tag{5}$$

$$u \to 0, \quad T \to T_\infty, \quad C^* \to C_\infty \quad \text{as} \quad y \to \infty, \quad t > 0 \tag{6}$$

The physical quantities of the model, that is, the local skin friction, local Nusselt number and local Sherwood number are given as:

$$C_f = \frac{2\tau_\omega t^{\frac{2n}{n+1}}}{\rho u_0^{2n-1} A^{2n}}, \quad Nu = \frac{q_\omega t^{\frac{1}{n+1}}}{\alpha(T_\omega - T_\infty)A}, \quad Sh = \frac{M_0 t^{\frac{1}{n+1}}}{DA(C_\omega - C_\infty)} \tag{7}$$

where $\tau_\omega = \Big(m\Big(-\frac{\partial u}{\partial y}\Big)^n\Big)_{y=0}$, $q_\omega = \Big[-\Big(\alpha + \frac{1}{\rho c_p} q_r\Big)\frac{\partial T}{\partial y}\Big]_{y=0}$, $M_0 = -D\Big(\frac{\partial C^*}{\partial y}\Big)_{y=0}$, and all other symbols are as defined in Table 1 below:

3 Analysis of the model

By employing the non-dimensional similarity variables below (Olajuwon [6]; Akaje et al., [27])

$$\eta = \frac{Ay}{t^{\frac{1}{n+1}}}, \quad \psi = u_0 f(\eta), \quad \theta = \frac{T - T_\infty}{T_\omega - T_\infty}, \quad C = \frac{C^* - C_\infty}{C_\omega - C_\infty}, \quad \text{and} \quad q_r = \frac{4\sigma^*}{3k^*}\frac{\partial T^4}{\partial y} \tag{8}$$

where A represents a constant and t is the time. The x and y components of the stream function are given as $u = \frac{\partial \psi}{\partial y}$, and $v = -\frac{\partial \psi}{\partial x}$ respectively.

After applying Equation 8 on Equations (2) - (7), the dimensionless momentum equation, energy equation, concentration equation, boundary conditions, local skin friction, local Nusselt number, and local Sherwood number are gotten as:

$$n(n+1)\vartheta^{1-n} u_0^{3n-1} f''(-f')^{n-1} + \frac{\eta\vartheta}{u_0^2} f' + Gr\theta cos\phi + GcC cos\phi + k_p f^n + Me^{-E\eta} = 0 \tag{9}$$

$$(n+1)\Big(\frac{3+4R}{3Pr}\Big)\theta'' + \eta\theta' + (n+1)Q\theta = 0 \tag{10}$$

$$\frac{1}{Sc}u_0^2(n+1)C'' + \eta C' - (n+1)\Gamma C = 0 \tag{11}$$

The dimensionless boundary conditions become:

$$f(0) = 1, \quad f'(0) = 1, \quad \theta(0) = 1, \quad C(0) = 1, \tag{12}$$

$$f(\infty) = 0, \quad \theta(\infty) = 0, \quad C(\infty) = 0 \tag{13}$$

The dimensionless local skin friction, local Nusselt number and local Sherwood number are derived as:

$$\frac{1}{2}C_f Re_n = (-f'^n(0)), \quad Nu = -\Big(1 + \frac{4}{3}Rd\Big)\theta'(0), \quad Sh = -C(0) \tag{14}$$

where $Rd = \frac{4\sigma^* T_\infty^3}{3k^* k}$ and $Re_n = \frac{t^{-\frac{n}{n+1}}\rho A^n u^{n-1}}{m}$.

4 Numerical solutions/Results

The dimensionless governing equations (9)-(11) along sides their boundary conditions in equation (12)-(13) are solved by employing shooting method embedded in MATLAB computational software. BV4C is only applicable for first order differential equations. Thus, the higher order derivatives in equations (9) - (11) and their boundary conditions (12) - (13) are converted to a system of first order differential equations as follows: Let

$$f = y_1, \quad f' = y_2, \quad \theta = y_3, \quad \theta' = y_4, \quad C = y_5, \quad C' = y_6 \tag{15}$$

Using the transformation in equation (15) on equations (9) – (13), we arrive at equations (16) –(20)

$$f'' = y_2' = \frac{-\Big[\frac{\eta\vartheta}{u_0^2}y_2 + Gry_3cos\phi + Gcy_5cos\phi + k_p y_1^n + Me^{-E\eta}\Big]}{n(n+1)\vartheta^{1-n}u_0^{3n-1}(-y_2)^{n-1}} \tag{16}$$

$$\theta'' = y_4' = \frac{-3Pr\Big[\eta y_4 + (n+1)Qy_3\Big]}{(3+4Rd)(n+1)} \tag{17}$$

$$C'' = y_6' = \frac{Sc\Big[(n+1)\Gamma y_5 - \eta y_6\Big]}{u_0^2(n+1)} \tag{18}$$

The appropriate boundary conditions are given as

$$y_1(0) = 1, \quad y_3(0) = 1, \quad y_5(0) = 1, \quad C(0) = 1, \tag{19}$$

$$y_1(\infty) = 0, \quad y_3(\infty) = 0, \quad y_5(\infty) = 0 \tag{20}$$

For numerical computations, the following constant values are used for fluid parameters. $\vartheta = 0.01$, $Gc = 3.0$, $\phi = \frac{\pi}{2}$, $M = 0.5$, $\Gamma = 0.1$, $Pr = 2.0$, $Sc = 0.6$, $Q = 0.05$, $Rd = 0.2$, $E = Gr = u_0 = k_p = 1.0$, and $n = 0.8$.

The numerical outcomes of the combine effects of these prominent fluid parameters on the velocity , temperature and concentration distributions are depicted graphically through figures 2 to 14 and in tabular form below:

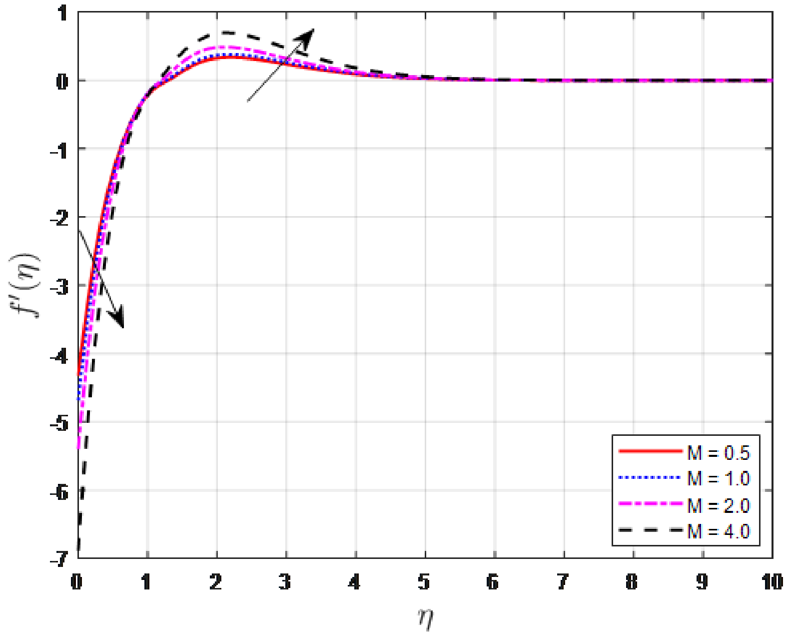

Figure 2: Effect of magnetic parameter M on velocity $f'(\eta)$ when $n = 0.8$

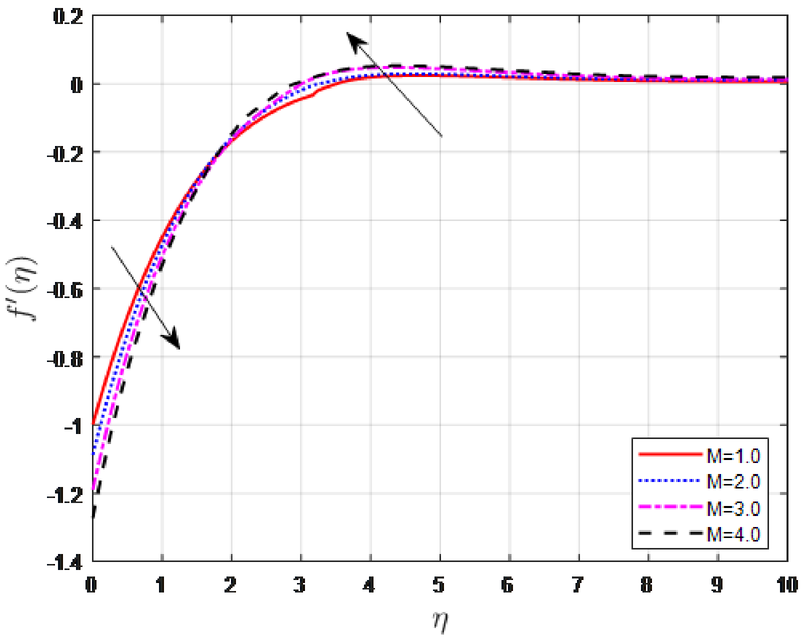

Figure 3: Effect of magnetic parameter M on velocity $f'(\eta)$ when $n = 1.2$

Table 1: Nomenclature

Parameter	Symbol	Expression
Constant	A	-
Uniform magnetic field strength	B_0	-
Dimensional concentration	C^*	-
Concentration at the wall	C_ω	-
Skin friction coefficient	C_f	$\frac{2\tau_\omega t^{\frac{2n}{n+1}}}{\rho u_0^{2n-1} A^{2n}}$
Specific heat at constant pressure	c_p	J kg^-1
Concentration away from the wall	C_∞	-
Electrical conductivity parameter	E	$\frac{\pi\nu}{l_0 u_0^2}$
Dimensionless velocity	f	-
Acceleration due to gravity	g	m/s^2
Mass Grashof number	Gc	$\frac{g\lambda_0\nu(C_\omega - C_\infty)}{u_0^3}$
Thermal Grashof number	Gr	$\frac{g\beta_0\nu(T_\omega - T_\infty)}{u_0^3}$
Thermal conductivity	k	$Wm^{-1}K^{-1}$
Rosseland mean absorption coefficient	k^*	m^{-1}
Porosity parameter	k_p	$\frac{\nu^2 u_0^n}{k_0 u_0^3}$
Consistency coefficient	m	-
Constants	m_0, m_1	-
Magnetic parameter	M	$\frac{\pi J_0 m_1 \nu}{8\rho u_0^3}$
Power-law exponent	n	-
Nusselt number	Nu	$\frac{q_\omega t^{\frac{1}{n+1}}}{\alpha(T_\omega - T_\infty)A}$
Prandtl number	Pr	$\frac{\rho c_p}{kA^2}$
Dimensional Heat source	Q_1	$\frac{Q_0\nu}{u_0^2 t}$
Dimensionless Heat generation/absorption parameter (Heat source)	Q	$\frac{Q_0\nu}{\rho c_p u_0^2}$
Heat flux	q_ω	$\left[-\left(\alpha + \frac{1}{\rho c_p} q_r\right)\frac{\partial T}{\partial y}\right]_{y=0}$
Radiative heat flux	q_r	$-\frac{4\sigma^*}{3k^*}\frac{\partial T^4}{\partial y}$
Radiation parameter	Rd	$\frac{4\sigma^* T_\infty^3}{kk^*}$
Reynolds'number	Re_n	$\frac{t^{-\frac{n}{n+1}}\rho A^n u^{n-1}}{m}$
Dimensional fluid temperature	T	K
Ambient temperature	T_∞	K
Time	t	s
Velocity components along the x-axis and y-axis	$u, \quad v$	-
Velocity on the wall of the stretching sheet	u_ω	m/s
Thermal diffusivity	α	$\frac{k}{\rho c_p}$
Dimensionless coordinate	η	-
Thermal expansion coefficient	β	-
Angle of inclination	ϕ	degree
Chemical reaction parameter	Γ	-
First order chemical reaction parameter	Γ_1	-
Grinberg term	-	$/frac\pi J_0 m_0 8\rho e^{-\frac{\pi y}{l}}$
Concentration expansion coefficient	λ	-
Viscosity coefficient	μ	$Kgm^{-1}s^{-1}$
Magnetic permeability	μ_0	-
Kinematic viscosity	ν	-
Fluid density	ρ	Kg/m^3
Dimensionless temperature	θ	-
Shear stress	τ_ω	-
Electrical conductivity	σ	-

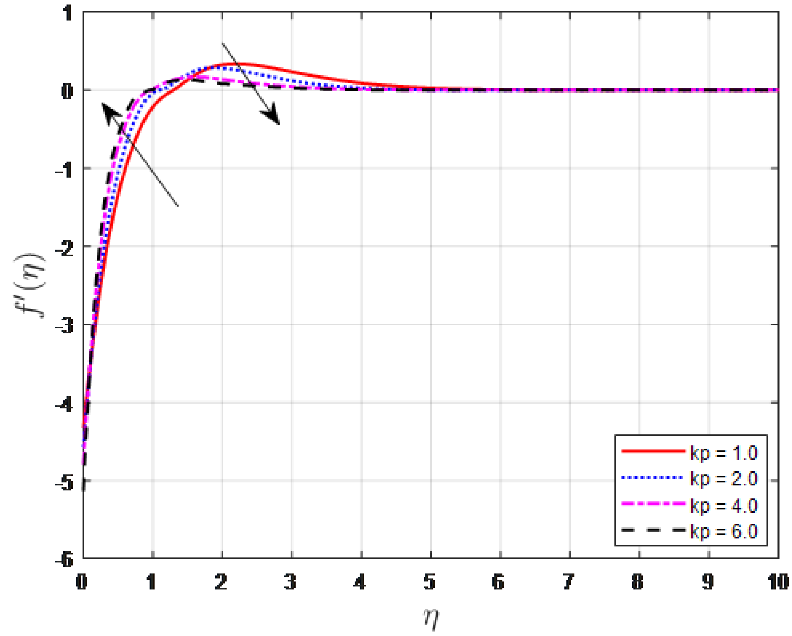

Figure 4: Effect of porosity parameter k_p on velocity $f'(\eta)$ when $n = 0.8$

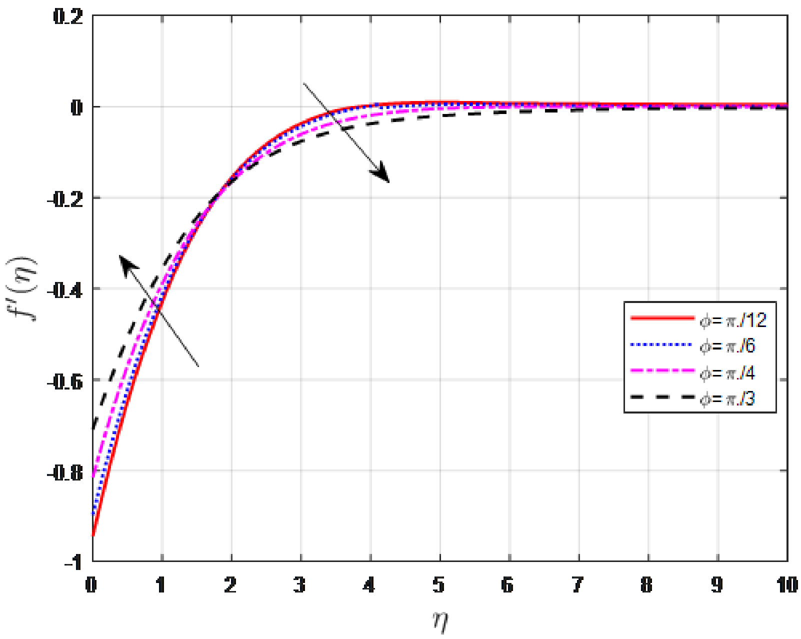

Figure 5: Effect of porosity parameter k_p on velocity $f'(\eta)$ when $n = 1.2$

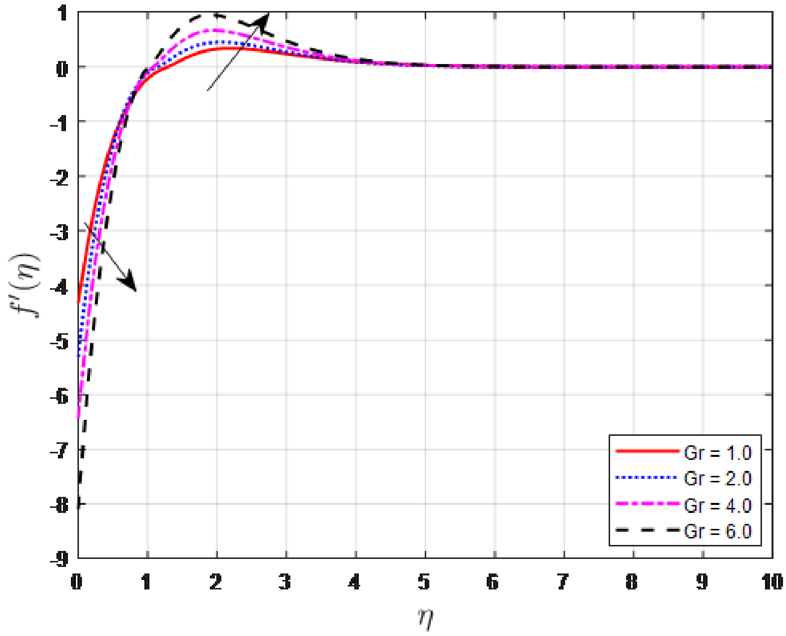

Figure 6: Effect of thermal Grashof number Gr on velocity $f'(\eta)$ when $n = 0.8$

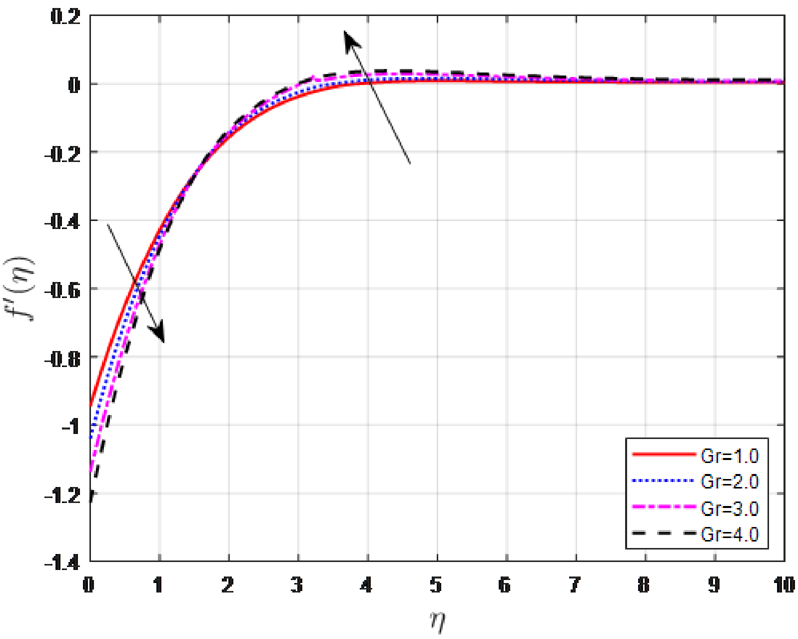

Figure 7: Effect of thermal Grashof number Gr on velocity $f'(\eta)$ when $n = 1.2$

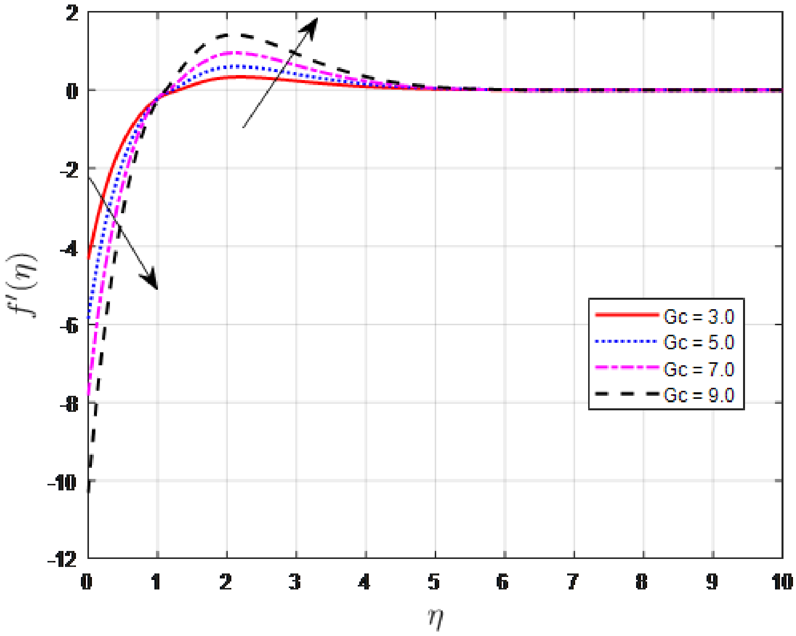

Figure 8: Effect of mass Grashof number Gc on velocity $f'(\eta)$ when $n = 0.8$

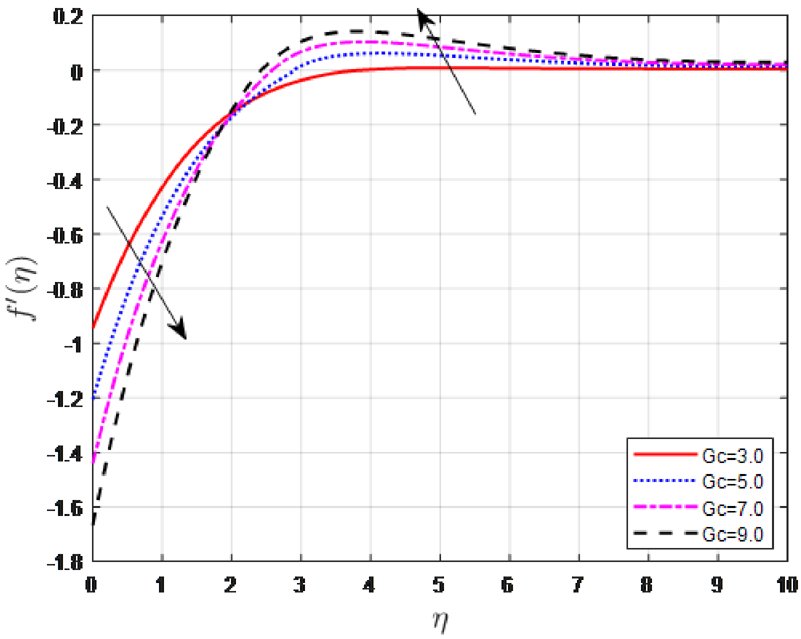

Figure 9: Effect of mass Grashof number Gc on velocity $f'(\eta)$ when $n = 1.2$

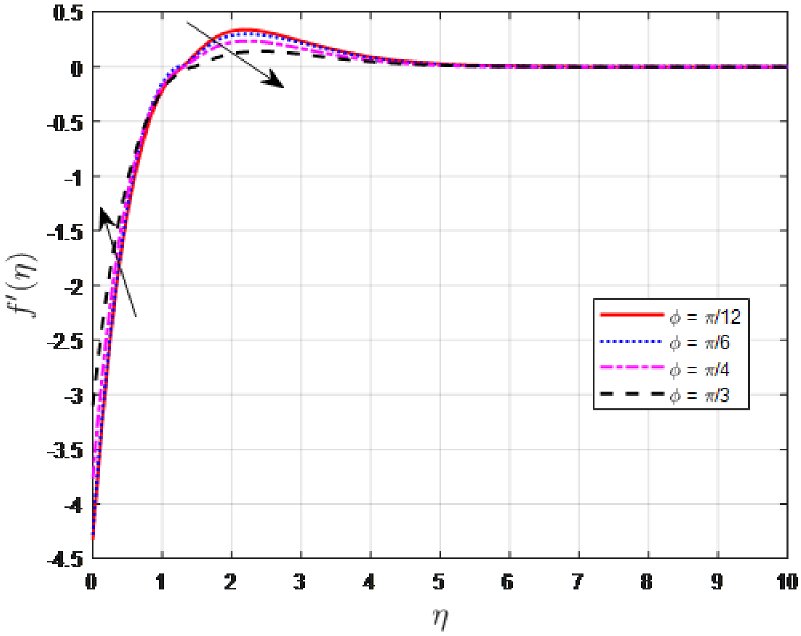

Figure 10: Effect of inclination angle ϕ on velocity $f'(\eta)$ when $n = 0.8$

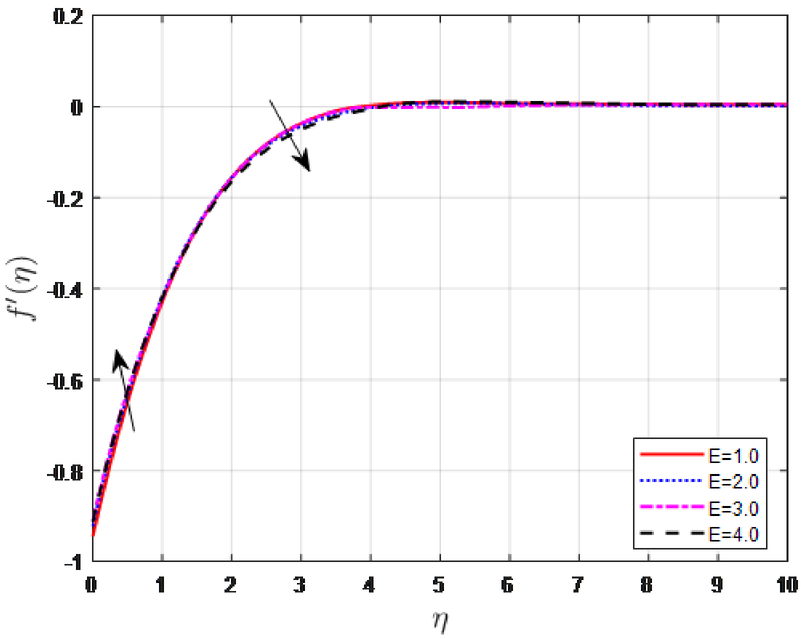

Figure 11: Effect of inclination angle ϕ on velocity $f'(\eta)$ when $n = 1.2$

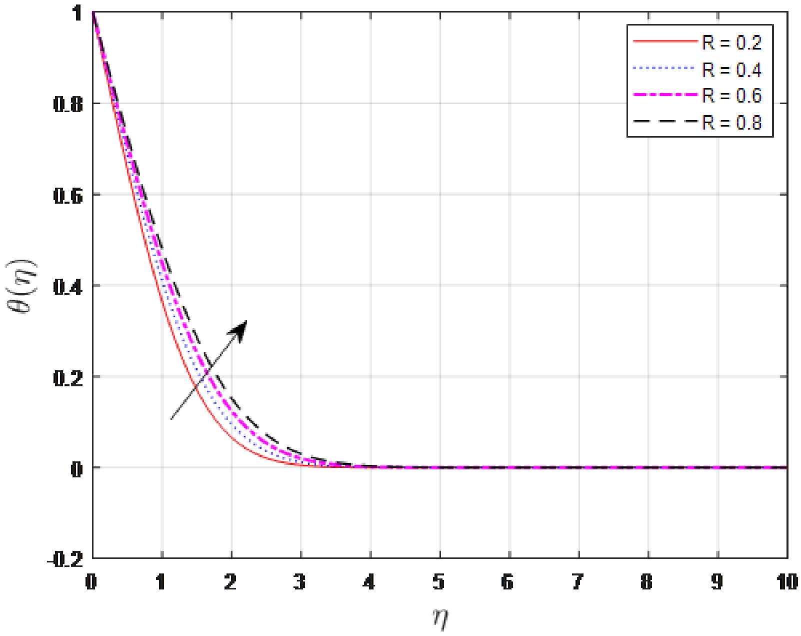

Figure 12: Effect of thermal radiation Rd on velocity $f'(\eta)$ when $n = 0.8$

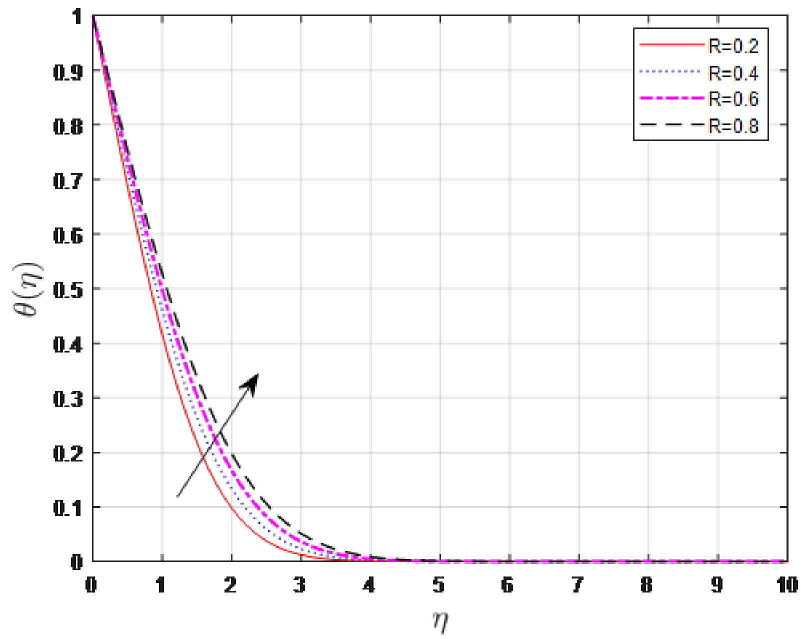

Figure 13: Effect of thermal radiation Rd on velocity $f'(\eta)$ when $n = 1.2$

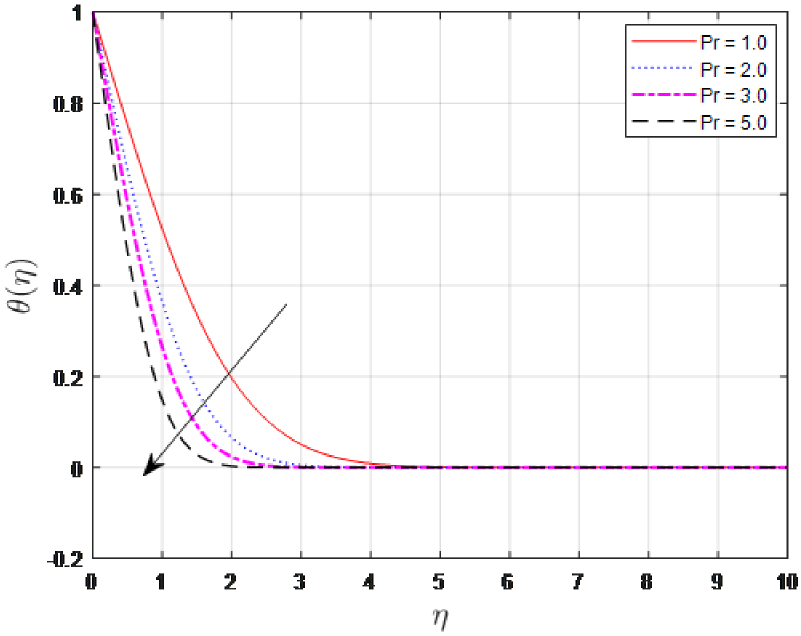

Figure 14: Effect of Prandtl number Pr on velocity $f'(\eta)$ when $n = 0.8$

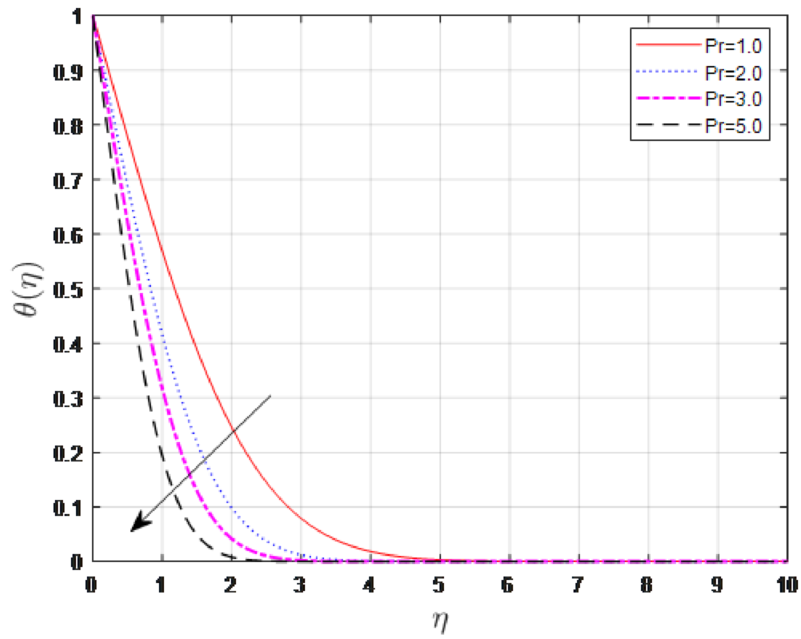

Figure 15: Effect of Prandtl number Pr on velocity $f'(\eta)$ when $n = 1.2$

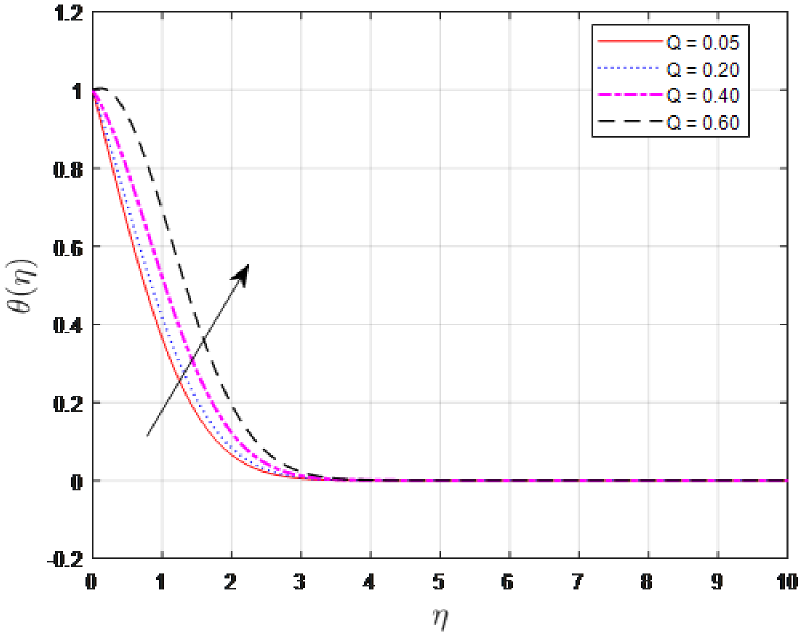

Figure 16: Effect of heat generation parameter Q on temperature $\theta(\eta)$ when $n = 0.8$

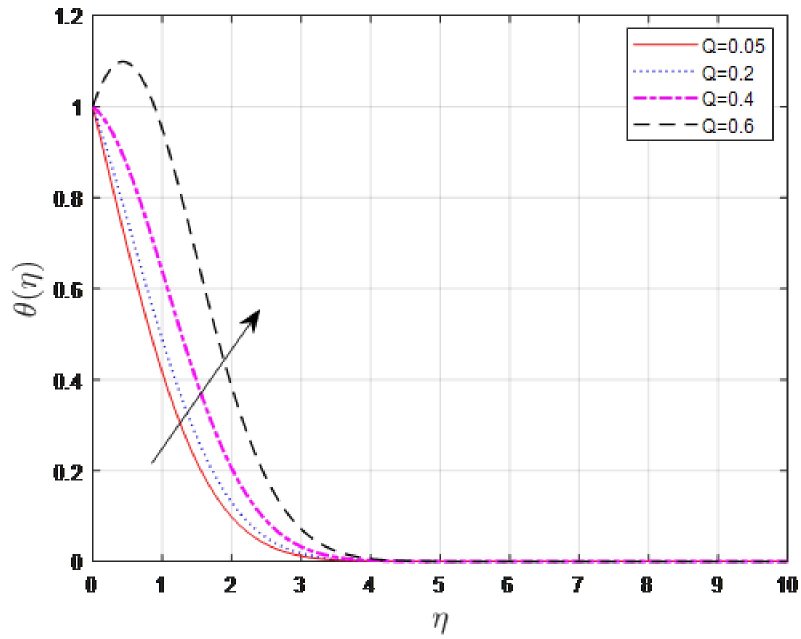

Figure 17: Effect of heat generation parameter Q on temperature $\theta(\eta)$ when $n = 1.2$

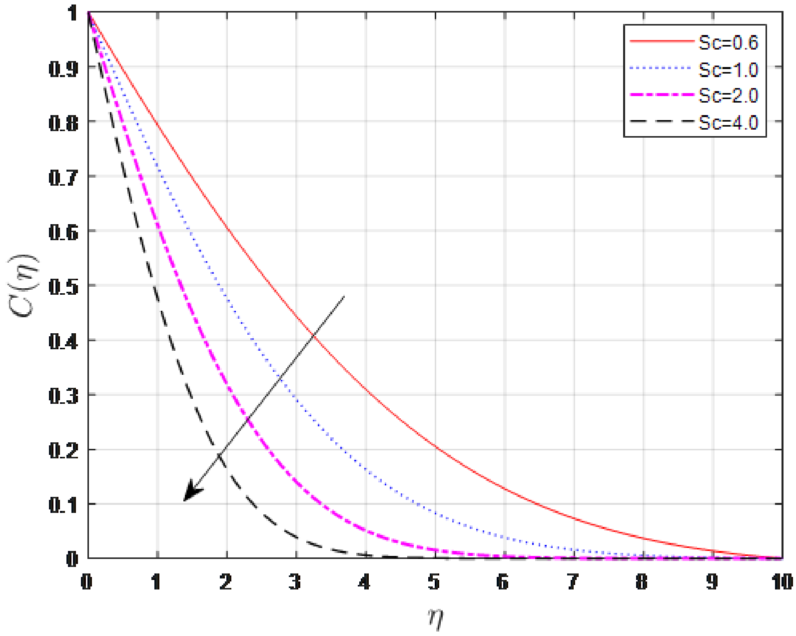

Figure 18: Effect of Schmidt number Sc on concentration $C(\eta)$ when $n = 0.8$

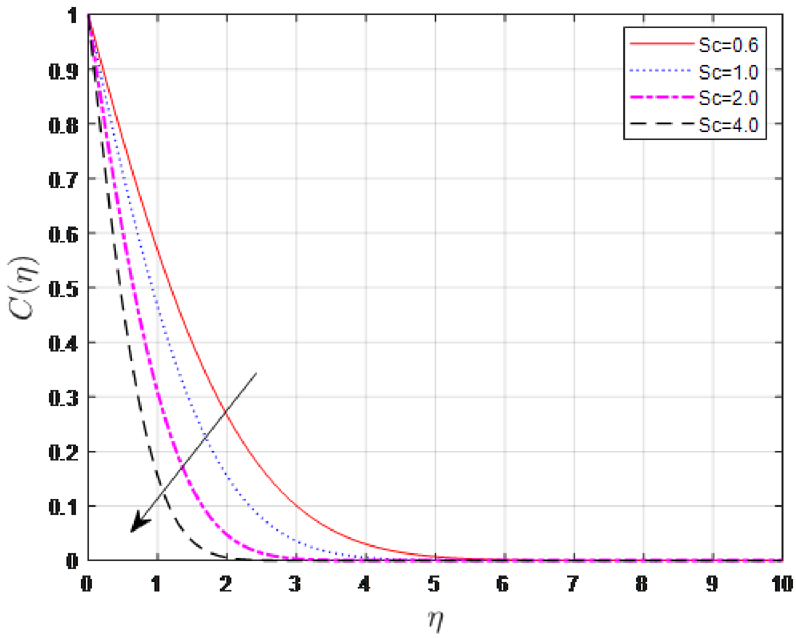

Figure 19: Effect of Schmidt number Sc on concentration $C(\eta)$ when $n = 1.2$

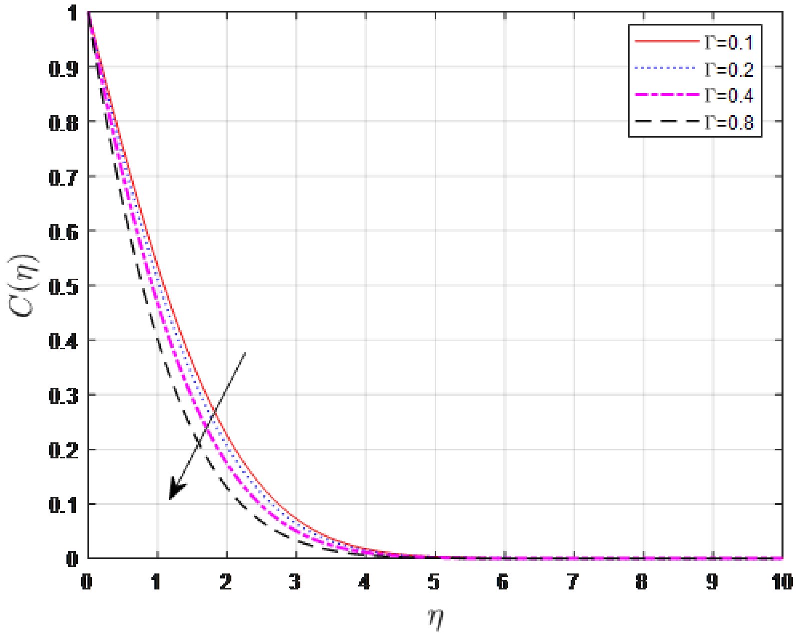

Figure 20: Effect of chemical reaction parameter Γ on concentration $C(\eta)$ when $n = 0.8$

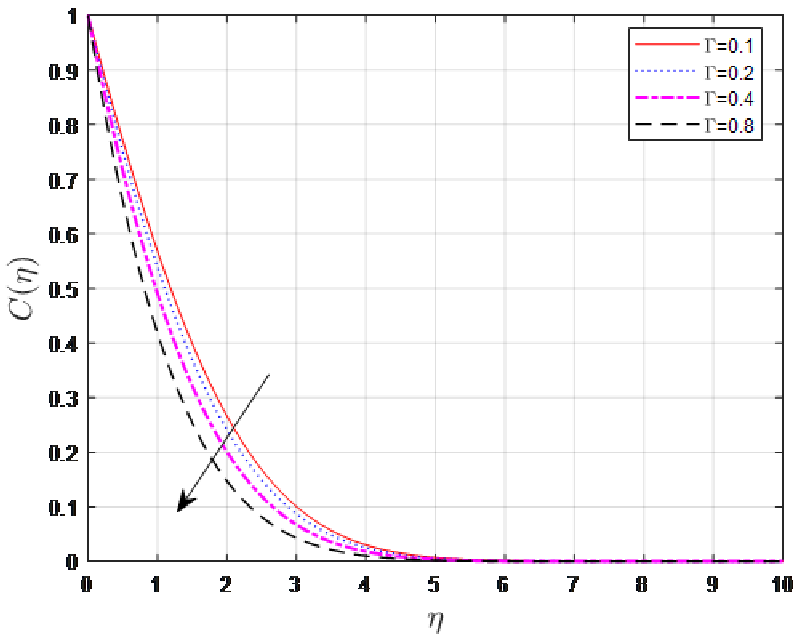

Figure 21: Effect of chemical reaction parameter Γ on concentration $C(\eta)$ when $n = 1.2$

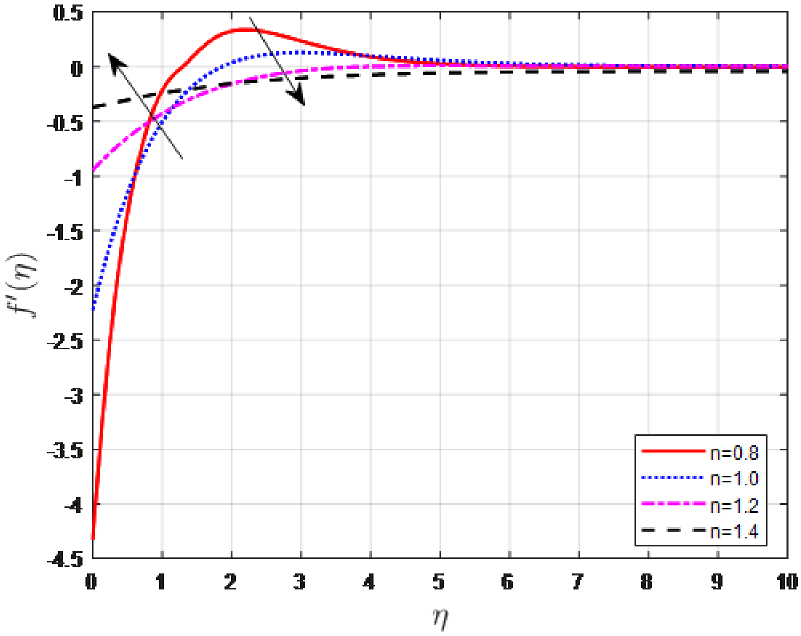

Figure 22: Effect of power-law exponent n on velocity $f'(\eta)$

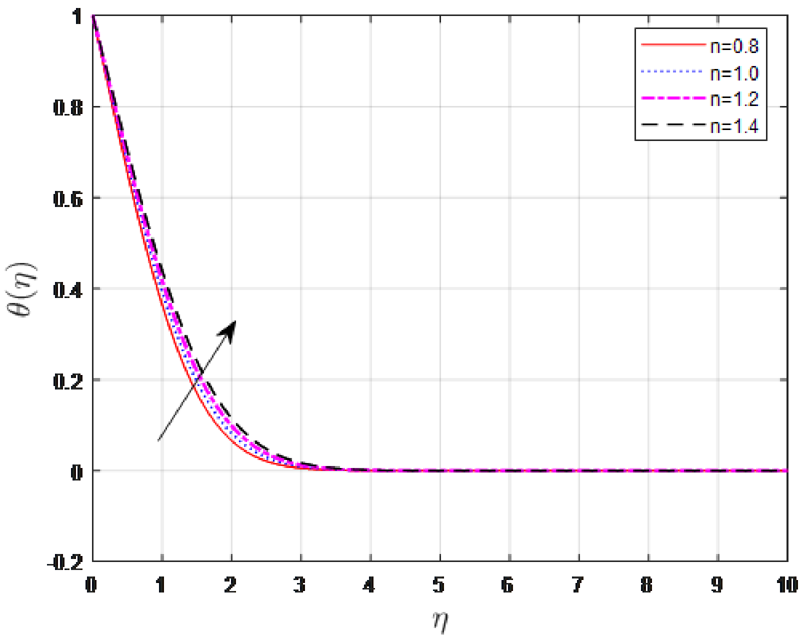

Figure 23: Effect of power-law exponent n on temperature $\theta(\eta)$

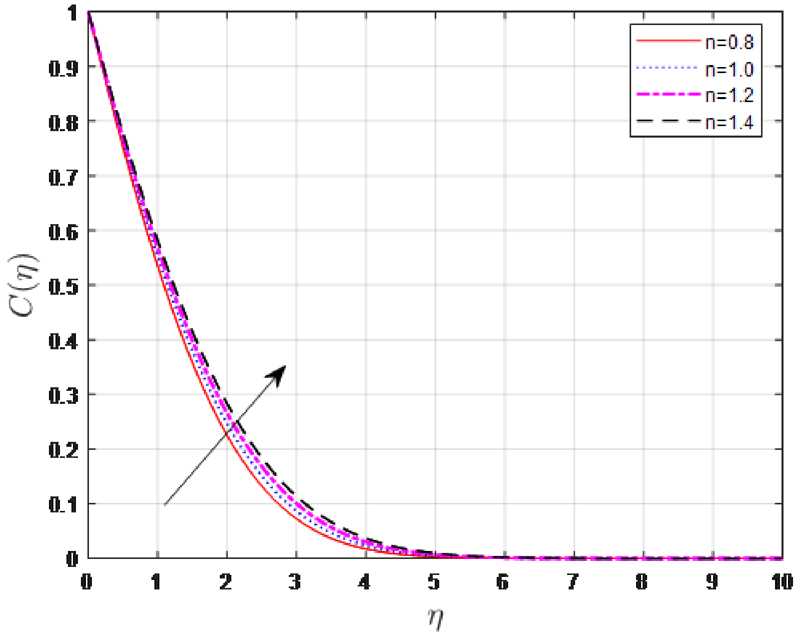

Figure 24: Effect of power-law exponent n on concentration $C(\eta)$

Table 2: Quantitative results of the skin friction coefficient, Nusselt number and Sherwood number for the pseudoplastic fluid ($n < 1$) when M, k_p, ϕ, Rd, Pr, Q, Sc, and Γ are varied

n	M	k_p	ϕ	R	Pr	Q	Sc	Γ	$\frac{1}{2}C_f \mathrm{Re}_n$	Nu	Sh
0.8	0.5	1.0	$\pi/12$	0.2	2.0	0.05	0.6	0.1	2.5739	0.8862	0.5158
	1.0								2.7262	0.8862	0.5158
	0.5	2.0							2.7236	0.8862	0.5158
		4.0							2.8293	0.8862	0.5158
		1.0	$\pi/6$						2.5738	0.8862	0.5158
			$\pi/4$						2.3279	0.8862	0.5158
			$\pi/12$	0.4					2.6931	0.9750	0.5158
				0.6					2.7132	1.0564	0.5158
				0.2	3.0				2.7107	1.0853	0.5158
					5.0				2.6869	1.4011	0.5158
					2.0	0.2			2.7931	0.6856	0.5158
						0.4			2.8075	0.3522	0.5158
						0.05	1.0		2.6312	0.8862	0.6658
							2.0		2.4593	0.8862	0.9416
							0.6	0.2	2.7272	0.8862	0.5667
								0.4	2.6518	0.8862	0.6589

Table 3: Quantitative results of the skin friction coefficient, Nusselt number and Sherwood number for the pseudoplastic fluid ($n > 1$) when M, k_p, ϕ, Rd, Pr, Q, Sc, and Γ are varied

n	M	k_p	ϕ	R	Pr	Q	Sc	Γ	$\frac{1}{2}C_f \mathrm{Re}_n$	Nu	Sh
1.2	0.5	1.0	$\pi/12$	0.2	2.0	0.05	0.6	0.1	0.8299	0.7891	0.4771
	1.0								0.9483	0.7891	0.4771
	0.5	2.0							0.9470	0.8965	0.4771
		4.0							1.0426	0.7891	0.4771
		1.0	$\pi/6$						0.7975	0.7891	0.4771
			$\pi/4$						0.7165	0.7891	0.4771
			$\pi/12$	0.4					0.8705	0.8682	0.4771
				0.6					0.8559	0.9406	0.4771
				0.2	3.0				0.8658	0.9664	0.4771
					5.0				0.7264	1.2476	0.4771
					2.0	0.2			0.8993	0.5602	0.4771
						0.4			0.8682	0.1493	0.4771
						0.05	1.0		0.7841	0.7891	0.6159
							2.0		0.7146	0.7891	0.8710
							0.6	0.2	0.8539	0.7891	0.5321
								0.4	0.7910	0.7891	0.6300

5 Discussions and conclusion

The illustration of the impact of magnetic parameter M on the velocity field of the power law fluid can be seen in Figure 2 and 3. The velocity gradient of the power law fluid is slowed down at the plate but rising away from the plate when the magnetic parameter is increased for both the pseudo-plastic non-Newtonian fluid and the dilatants non-Newtonian fluid. This is because the Lorentz force or resistance force generated by the magnetic parameter is more pronounced at the wall, thereby impeding the fluid flow there but less pronounced away from it. In Figure 4 and 5, the influence of porosity parameter k_p on the boundary layer flow of the power law fluid is represented for the pseudo-plastic and dilatants fluids. The graph reveals a decline in the flow field and momentum boundary-layer thickness away from the plate for the non-Newtonian fluids which is due to the presence of the permeable materials. Thus, a rise in porosity parameter resulted in the deceleration of the power law fluid flow as depicted in the graph. Figure 6 and 7 shows the behaviour of the fluid flow field for power law fluid when $0 < n < 1$ and $n > 1$ as the thermal Grashof number Gr is varied. It is noticed that for both the pseudo-plastic and dilatants fluids, an enhanced thermal Grashof number causes the temperature profile of the power law fluid to rise as the fluid move away from the plate. The direct relationship between fluid temperature and thermal Grashof number in a convection process might have responsible for this. An augmented thermal Grashof number lead to temperature rise and decrease in density of the fluid which increases the fluid acceleration eventually. In Figure 8 and 9, the correlation between the mass Grashof number Gc, and fluid flow for pseudo-plastic non-Newtonian fluid and dilatant non-Newtonian fluid is shown. We see that an increase in mass Grashof number widen the thickness of the velocity field as the power law fluid move away from the plate. It is observed that mass Grahsof when increase, increases the fluid concentration gradient and consequently the buoyancy force. The influence of the inclination angle ϕ, on the velocity profile of the power law fluid is depicted in Figure 10 and 11. The chart reveals that an increase in the inclination angle increases the fluid flow near the plate only for the pseudo-plastic fluid and dilatant fluid. The velocity of the fluid decelerates as the fluid move away from the plate. Figure 12 and 13 shows the effect of radiation parameter Rd, on the temperature profile of power law fluid for the pseudo-plastic fluid and dilatants fluid. An augmented radiation parameter raises the temperature of the fluid as portray by the chart for both fluids. A higher radiation parameter raises the kinetic energy of the fluid molecules due to heat which in turn induced intense molecular collisions and thus leads to fluid temperature rise. The impact of Prandtl number Pr, on the thermal field of a power law fluid for the cases when the exponent is $0 < n < 1$ and $n > 1$ is seen in Figure 14 and 15. The temperature inside the boundary layer decreases with an increase in Prandtl number for the two cases. Thermal diffusivity decreases with rising Prandtl number, which means that fluid particles migrate from the hot to the cold side more slowly. As a result, the temperature profile of power law fluid is reduced. Figures 16 and 17 illustrate how the heat generation/absorption parameter Q, affects the pseudo-plastic and dilatant temperature distributions. It is observed that an enhanced heat generation/absorption parameter raises the temperature profile of the power law fluid for both cases.

Figure 18 and 19 illustrates the effect of Schmidt number Sc on the concentration profiles of the power law fluid. It is clear that an increase in value of Schmidt number results in a large drop in both the boundary-layer thickness and species concentration for both the pseudo-plastic non-Newtonian fluid and the dilatant non-Newtonian fluid. This is as result of the fact an advanced Schmidt number increases mass diffusion over the momentum in the convective fluid flow. The significance of chemical reaction parameter Γ in the boundary layer of the pseudo-plastic and dilatant fluids is elucidated on the concentration profile in Figure 20 and 21. It is observed that the power law fluid concentration shrinks when enriching the chemical reaction parameter for the two classes of non-Newtonian fluids considered. Analysis on Power Law Exponent Parameter The significance of the power law exponent parameter on the velocity, temperature, and concentration profiles is carried out on Figures 22, 23 and 24 respectively. Figure 22 reveals the influence of the higher exponent parameter on the velocity distribution of the power law fluid. It is observed that dilatant fluid flows faster than Newtonian fluid and pseudo-plastic fluid, respectively, at the boundary but opposite behavior is observed away from the boundary. This implies that the augmented exponent parameter accelerates the fluid flow only at the plate but decelerates it away from the plate. Figures 23 and 24 illustrate the behaviour of both the temperature and concentration profiles with respect to the variation of the power law exponent parameter. It is observed that there is a direct relationship between the exponent parameter and the temperature and concentration fields. An increase in the exponent parameter increases both the temperature profile and the concentration profile. The dilatant fluid has the most pronounced improvement, followed by Newtonian fluid and then pseudo-plastic fluid on the temperature and concentration profiles.

The computational outcomes of the three physical quantities skin friction Nusselt number , and Sherwood number for the pseudoplastic fluids are presented in Table 2 for various entries of the magnetic parameter, the porosity parameter, the inclination angle parameter, the radiation parameter, the Prandtl number , the heat generation/absorption parameter, the Schmidt number, and the chemical reaction parameter. The impact of the magnetic, porosity, and inclination parameters is much more noticeable on the skin friction. Table 2 illustrates that the skin friction coefficient increases as the magnetic parameter, and the porosity parameter increase but decreases with an advanced inclination angle parameter. The reaction of the Nusselt number to different values of the radiation parameter, the Prandtl number, and, the heat generation/absorption parameter is pronounced in Table 2. It is observed that an augmented radiation parameter and heat generation/absorption parameter accelerate the rate of heat transfer while a higher Prandtl number retards it. Additionally, the varying Schmidt number and the chemical reaction parameter prominently affect the Sherwood number as demonstrated in Table 2. The rate of mass diffusion declines with the exaggerated Schmidt number and the chemical reaction parameter.

Table 3 presents the quantitative results for different values of the magnetic parameter, the porosity parameter, the inclination angle parameter, the radiation parameter, the Prandtl number , the heat generation/absorption parameter, the Schmidt number, and the chemical reaction parameter on the skin friction the Nusselt number, and the Sherwood number for the dilatant fluid. Behaviour of skin friction with different values of the magnetic parameter, the porosity parameter, and the inclination angle parameter indicates that the flow rate improves with the augmented magnetic parameter and porosity parameter. In contrast, the higher inclination angle parameter impedes the flow rate. The effect of the radiation parameter, the Prandtl number, and the heat generation/absorption parameter from Table 3 shows that the enriched radiation parameter, heat generation/absorption parameter, and Prandtl number retard the heat transfer rate. Furthermore, the mass diffusion rate is greatly reduced by the higher Schmidt number and the chemical reaction parameter.

The summary of the investigation on the combined effects of heat generation/absorption parameter, thermal radiation parameter, inclination angle, mass Grashof number, thermal Grashorf number and chemical reaction parameter on the velocity, temperature and concentration profiles of the convective heat and mass transfer in a power law fluid over an inclined Riga plate is hereby itemized below.

- The velocity of the power law fluid declines at the plate but rises away from the plate when the magnetic parameter, the thermal Grahsof number, or the mass Grahsof is enhanced for both the pseudoplastic fluid and dilatant fluid.

- The velocity profile of both the pseudoplastic fluid and dilatant fluid accelerates near the plate only for a higher value of the power-law exponent, porosity parameter, or inclination angle.

- An augmented power-law exponent, radiation parameter, or heat generation/absorption raises the temperature profile of the pseudoplastic fluid and dilatant fluid.

- The temperature inside the boundary layer decreases with an increase in Prandtl number for the pseudoplastic fluid and dilatant fluid.

- The power law fluid concentration boundary-layer thickness shrinks when enriching either the chemical reaction parameter or Schmidt number for both the pseudoplastic fluid and dilatant fluid meanwhile an enhancement of the power-law exponent increases the concentration profile for the both fluids.

References

[1] Schlichting, H. (1979). Boundary Layer Theory. McGraw-Hill, New York.

[2] Zhang, H., Zhang, X. and Zheng, L. (2007). Numerical study of thermal boundary layer on a continuous moving surface in power law fluids. J. Therm. Sci. 16(3), 243–247.

[3] Bharti, R.P., Chhabra, V. and Eswaran, D. (2007). Steady forced convection heat transfer from a heated circular cylinder to power-law fluids. Int. J. Heat Mass Transfer 50, 977–990.

[4] Hassan, I.A., Abdullah, A.A. and Gorla, R.S.R. (1998). Flow and heat transfer in a power law fluid over a non-isothermal stretching sheet, Math. Comput. Model. 28, 105–116.

[5] Donald P.A. (2002). On the flow of power law fluid over a stretching sheet techniques and solutions. Acta Mech. 156, 13–27.

[6] Olajuwon, B.I. (2009). Flow and natural convection heat transfer in a power law fluid past a vertical plate with heat generation. International Journal of Nonlinear Science 7(1), 50-56.

[7] Olajuwon, B.I. and Oyelakin, I.S. (2012). Convection heat and mass transfer in a power law fluid with non-constant relaxation time past a vertical porous plate in the presence of thermo and thermal diffusion. Journal of Theoretical and Applied Mechanics, Sofia 42(4), 53–74. DOI: 10.2478/v10254-012-0020-1

[8] Chamkha, A.J. and Khaled, A.A. (2012). Similarity solutions for hydromagnetic simultaneous heat and mass transfer by natural convection from an inclined plate with heat generation and absorption. Heat and Mass Transfer 37(2-3), 117–23.

[9] Chamkha, A.J. (2004). Unsteady MHD convective heat and mass transfer past a semi-finite vertical permeable moving plate with heat absorption. Int J Eng Sci. 42(2), 217–30.

[10] Asimoni, M.N., Mohammad, N.F., Kasim, A.M. and Sha, E.S. (2020). MHD mixed convective flow of power-law nanofluid in a lid-driven cavity with heat generation and chemical reaction effects: Buongiorno's Model. Malaysian J. Fund. Appl. Sci. 16(5), 576-584.

[11] Reddy, S.H., Naidu, K.K., Babu, D.H., Narayana, P.V. and Raju, M.C. (2020). Significance of chemical reaction on MHD near stagnation point flow towards a stretching sheet with radiation. SN Appl Sci. 2(11), 1822-1831.

[12] Nandkeolyar, R., Das, M. and Sibanda, P. (2013). Exact solutions of unsteady MHD free convection in a heat absorbing fluid flow past a flat plate with ramped wall temperature. Bound Value Probl. 2013(1), 247-257.

[13] Gailitis, A. and Lielausis, O. (1961). On possibility to reduce the hydrodynamics resistance of a plate in an electrolyte. Appl. Magnetohydrodyn. Rep. Phys. Inst. Riga 12, 143–146.

[14] Ahmad, R., Mustafa, M. and Turkyilmazoglu, M. (2017). Buoyancy effects on nanofluid flow past a convectively heated vertical Riga-plate: A numerical study. International Journal of Heat and Mass Transfer 111, 827–835.

[15] Pantokratoras, A. and Magyari, E. (2009). MHD free-convection boundary-layer flow from a Riga-plate. J. Eng. Math. 64, 303–315.

[16] Magyari, E. and Pantokratoras, A. (2011). Aiding and opposing mixed convection flows over the Riga plate. Commun. Nonlinear Sci. Numer. Simul. 16, 3158–3167.

[17] Hayat, T. Abbas, T., Ayub, M., Farooq, M. and Alsaedi, A. (2016). Flow of nanofluid due to convectively heated Riga plate with variable thickness. J. Mol. Liq. 222, 854–862.

[18] Ramesh, G.K., Roopa, G.S., Gireesha, B.J., Shehzad, S.A. and Abbasi, F.M. (2017). An electromagneto-hydrodynamic flow of Maxwell nanoliquid past a Riga plate: a numerical study. J. Braz. Soc. Mech. Sci. Eng. 2017, 1–8. https://doi.org/10.1007/s40430- 017-0900-z.

[19] Prasannakumara, B.C., Shashikumar, N.S. and Ramesh, G.K. (2020). Magnetohydrodynamic flow of dusty fluid over Riga plate with deforming isothermal surfaces with convective boundary condition, Songklanakarin J. Sci. Technol. 42(3), 487–495.

[20] Rasool, R. and Zhang, T. (2019). Characteristics of chemical reaction and convective boundary conditions in Powell-Eyring nanofluid flow along a radiative Riga plate. Heliyon 5, e01479, https://doi.org/10.1016/j.heliyon.2019.

[21] Hayat, T. Qayyum, S., Shehzad, S.A. and Alsaedi, A. (2017). Simultaneous effects of heat generation/absorption and thermal radiation in magnetohydrodynamic (MHD) flow of Maxwell nanofluid towards a stretched surface, Results Phys. 7, 562–573.

[22] Rashad, A.M. (2017). Impact of thermal radiation on MHD slip flow of ferrofluid over a non-isothermal wedge. J. Magn. Magn. Mater. 422, 25–31.

[23] Lopez, A., Ibanez, G., Pantoja, J., Moreira, J. and Lastre, O. (2017). Entropy generation analysis of MHD nanofluid flow in a porous vertical microchannel with nonlinear thermal radiation, slip flow and convective-radiative boundary conditions. Int. J. Heat Mass Tran. 107, 982–994.

[24] Khan, S.A., Hayat, T. and Alsaedi, A. (2022). Simultaneous features of Soret and Dufour in entropy optimized flow of Reiner-Rivlin fluid considering thermal radiation. Int. Commun. Heat Mass Tran. 137 (2022), https://doi.org/10.1016/j.icheatmasstransfer.2022.106297.

[25] Bilal, M., Sagheer, M. and Hussain, S. (2018). Numerical study of magnetohydrodynamic and thermal radiation on Williamson nanofluid flow over a stretching cylinder with variable thermal conductivity. Alex. Eng. J. 57, 3281–3289.

[26] Daniel, Y.S., Aziz, Z.A. Ismail, Z. and Salah, J. (2019). Impact of thermal radiation and viscous dissipation on the time-dependent and chemically reactive magnetohydrodynamic (MHD) flow. J. King Saud University– Sci. 31, 804-814.

[27] Akaje, T. W., Taiwo, M. A., Olajuwon, B. I., Raji, M. T. and Akinleye, S. A. 2023. Double-Diffusive Nonlinear buoyancy force significance on free convective chemically reacting fluid flow past vertical Riga plate. Journal of Advanced Research in Fluid Mechanics and Thermal Sciences 105(1), 59–75.